

Article

Laser Scanning Method for Time-Resolved Measurements of Wavefront Distortion Introduced by Active Elements in High-Power Laser Amplifiers

Alyona O. Kuptsova ^{1,2}, Gleb V. Kuptsov ^{1,3}, Vladimir A. Petrov ^{1,3}, Victor V. Atuchin ^{4,5,6,*}
and Victor V. Petrov ^{1,2,3}

- ¹ Institute of Laser Physics, The Siberian Branch of the Russian Academy of Sciences, Pr. Lavrentyev, 15-B, Novosibirsk 630090, Russia; aokupts@gmail.com (A.O.K.); kuptsov.gleb@gmail.com (G.V.K.); petrov.nstu@gmail.com (V.A.P.); vpetv@laser.nsc.ru (V.V.P.)
 - ² Department of Physics, Novosibirsk State University, 2 Pirogov Str., Novosibirsk 630090, Russia
 - ³ Faculty of Physical Engineering, Novosibirsk State Technical University, 20 Prospekt K. Marksa, Novosibirsk 630073, Russia
 - ⁴ Laboratory of Optical Materials and Structures, Institute of Semiconductor Physics, The Siberian Branch of the Russian Academy of Sciences, Novosibirsk 630090, Russia
 - ⁵ Research and Development Department, Kemerovo State University, Kemerovo 650000, Russia
 - ⁶ Department of Industrial Machinery Design, Novosibirsk State Technical University, Novosibirsk 630073, Russia
- * Correspondence: atuchin@isp.nsc.ru

Abstract: A novel method was proposed for the experimental investigation of wavefront distortion introduced to amplified radiation by pumped active elements in high-power laser amplifiers. The method is based on the simultaneous measurement of temperature distribution and the distribution of population density of the excited laser level in active elements. The underlying theory of the technique was presented; various factors affecting the accuracy of wavefront distortion determination were analyzed. The method was tested to study the wavefront distortion and the depolarization of radiation introduced by the Yb:YAG active element of a cryogenically cooled laser amplifier with high-power diode pumping. The focal length of the thermal lens was 0.40 ± 0.03 and 0.47 ± 0.05 m for the horizontal and vertical planes, respectively. The focal length of the electron lens was two orders of magnitude larger. The maximum value of losses induced by depolarization was 8.5%.

Keywords: thermo-optic effects; wavefront distortion; high-power amplifiers; laser thermometry; laser scanning method



Citation: Kuptsova, A.O.; Kuptsov, G.V.; Petrov, V.A.; Atuchin, V.V.; Petrov, V.V. Laser Scanning Method for Time-Resolved Measurements of Wavefront Distortion Introduced by Active Elements in High-Power Laser Amplifiers. *Photonics* **2024**, *11*, 748. <https://doi.org/10.3390/photonics11080748>

Received: 16 July 2024
Revised: 3 August 2024
Accepted: 7 August 2024
Published: 9 August 2024



Copyright: © 2024 by the authors. Licensee MDPI, Basel, Switzerland. This article is an open access article distributed under the terms and conditions of the Creative Commons Attribution (CC BY) license (<https://creativecommons.org/licenses/by/4.0/>).

1. Introduction

Currently, significant efforts are devoted to the creation and development of laser systems with both high pulse energy and a high pulse repetition rate. In many cases, such systems include amplifiers based on media doped with Yb³⁺ ions. This is due to the fact that Yb³⁺ ions have a low quantum defect of about 9%. In addition, many widely used active media, such as Yb:YAG, Yb:CaF₂, Yb:YLF [1,2], and other materials doped with Yb³⁺ ions, have good thermal conductivity, which increases significantly when the active element is cooled to cryogenic temperatures. Nevertheless, it is not possible to avoid the negative influence of thermal effects if the average pump radiation power is high enough. There are methods for a further decrease in a thermal load on active elements, for example, the movement of a pumped region in an active medium [3] or the application of several spatially separated slabs with different doping levels [4]. Another approach is the application of active elements with an ion doping concentration gradient in the direction of pump propagation. Gradient doping makes it possible to optimize the temperature

distribution in the active element, thus reducing a thermally induced wavefront distortion of the amplified radiation [5].

In laser systems with high pump radiation power, changes in the wavefront of the amplified radiation in the active elements lead to the appearance of pump-induced lenses [6,7] as well as to the depolarization of radiation [8,9]. These effects are especially detrimental in the case of multielement and multipass systems. The wavefront distortion of amplified radiation limits the output energy and the maximum reachable diameter of the focused radiation, which reduces the peak power and intensity [10,11]. Beam wavefront has a great influence on the performance of coherent beam combining [12]. The compensation of distortion caused by pumping the active element in laser systems is very important when scaling to multi-kilowatt average power levels. Taking this into account, wavefront distortion is necessary when developing the element base of a laser system [5] and tailoring pump and injection radiation parameters [13].

Typically, a Shack–Hartmann sensor [14–16] is used to measure wavefront distortion. This is a well-known, simple, and commercially available device. There are also wavefront measurement sensors based on lateral shearing interferometry [17]. Research using interferometers [18,19] is also common. For these approaches, the stability of the probe laser beam wavefront and intensity is most important. To separate the processes of wavefront distortion and the processes of changes in the spatial distribution of radiation intensity due to amplification or absorption, it is necessary to use probe laser radiation that is not absorbed or amplified in the active medium. The wavelength of the scanning radiation must also be in accordance within the spectral range for which the dielectric coatings of the optical elements are designed. Since the parameters of the medium and introduced distortion are wavelength-dependent, it is preferable to carry out the study at the amplification wavelength. In the case of measurements using interferometric methods, the disadvantage is also the complex setup and sensitivity to a drift of various mechanical units of the system [20]. Mechanical issues are especially significant in high-power laser systems due to the operation of the cooling system of the active elements.

If high stability of radiation parameters is required, it is also necessary to separate the contributions of various mechanisms in order to compensate them. However, in most cases, the methods discussed above do not allow decomposing the change in the refractive index caused by the thermal effects and polarizability difference in the excited and ground states of the active ions.

Wavefront distortion in pumped active elements can be calculated from the experimentally determined distribution of temperature and population density of the upper laser level in the active element [18,21]. On the one hand, with such a calculation, the results' accuracy depends on the accuracy of the laser and thermophysical characteristics of the medium. On the other hand, such a study makes it possible to distinguish between the thermal contribution to the change in the refractive index and the electronic one. In addition, such a calculation essentially complements the experimental studies of the pump radiation effect on the active medium. Such experimental studies are necessary to verify numerical models of temperature distribution and radiation amplification in active elements and estimate the quality of the thermal contact between the active element and the heat sink.

Thus, progress in the development of modern laser systems with high radiation power requires the development of new methods for studying the interaction of pump radiation, active medium, and amplified radiation. Currently, one of the directions of research is the development of novel techniques applicable in the case of cryogenic cooling, for the experimental study of temperature distribution in active elements and distortion of the wavefront of amplified radiation [21,22].

In this work, a laser scanning method was proposed for a simultaneous time-resolved study of the temperature distribution and the upper level population density in the active element of a high-power laser amplifier. The accuracy of the method was analyzed. The method was applied to study the wavefront distortion in a crystalline Yb:YAG active mirror of a cryogenically cooled multi-disk laser amplifier with a diode pump per element up

to 200 W [13]. The thermal and electronic contributions to optical path difference (OPD) profiles introduced by the pumped active elements to the wavefront of amplified radiation were experimentally determined and analyzed.

2. Laser Scanning Method

There are two contributions to the distortion of radiation wavefront in active elements. Thermal contribution ($\Delta l_{r,\theta}^{(th)}$) is associated with a temperature gradient in an active element, and electronic contribution ($\Delta l^{(el)}$) occurs because of a change in the polarizability of excited dopant ions. Thermal contribution to the change in the optical path length for radiation components with radial and tangential polarizations are different and are indicated by r and θ , respectively. OPD can be calculated with respect to any region of an active element. So, the center of a pumped area in an active element (x_0, y_0) is chosen. For the calculation of wavefront distortion caused by the temperature gradient in an active element, a common approach is the application of the plane strain approximation (for thin rods) and the plane stress approximation (for thin disks). Thus, the plane stress approximation is valid for the case of active elements in the form of active mirrors, which are often used in laser amplifiers with both high average and high peak power levels. The electronic contribution to OPD and thermal contribution calculated in the plane stress approximation can be described by the following formulae [23,24]:

$$\Delta l_{r,\theta}^{(th)}(x, y) = L \cdot \left[\chi^n(x, y) + \chi^{bg}(x, y) + \chi_{r,\theta}^{pe}(x, y) \right] \cdot \left(\overline{T(x, y)} - T_0 \right);$$

$$\chi^n = \left(\frac{\partial n}{\partial T} \right)_{\epsilon=0} (T(x, y)); \tag{1}$$

$$\chi^{bg} = (n_0 - 1) \cdot (1 + \nu) \cdot \alpha_T(T(x, y));$$

$$\chi_{r,\theta}^{pe} = 2 \cdot n_0^3 \cdot \alpha_T(T(x, y)) \cdot C_{r,\theta},$$

$$\Delta l^{(el)}(x, y) = \frac{2\pi \cdot (n_0^2 + 2)^2}{9n_0} \cdot \Delta p \cdot L \cdot N \tag{2}$$

where x, y are the Cartesian coordinates in the plane perpendicular to the z -axis; L is the optical path length in an active element, m; $\left(\frac{\partial n}{\partial T} \right)_{\epsilon=0} (T)$ is the partial derivative of refractive index with respect to temperature taken at a zero strain, K^{-1} ; n_0 is the refractive index of the medium before pumping is turned on; $\alpha_T(T)$ is the thermal expansion coefficient, K^{-1} ; $C_{r,\theta}$ are photoelastic constants for radiation components with radial and tangential polarizations, respectively; ν is Poisson's ratio; $\overline{T(x, y)} - T_0 = \frac{1}{L} \int_0^L [T(x, y, z) - T(x_0, y_0, z)] dz$ is the temperature difference averaged along the beam propagation axis (z -axis), K; Δp is the polarizability difference in dopant ions in the excited and ground states, m^3 ; and $N(x, y)$ is the population of the excited laser state, ions/ m^3 .

In Equation (1), different terms account for different mechanisms involved into the formation of wavefront distortion of amplified radiation. The first term is associated with the refractive index dependence on temperature; the term with χ^{bg} takes into account the end faces bulging caused by the thermal expansion of the active medium. The term with χ^{pe} is related to thermal stresses in the medium resulting in the induced birefringence due to the photoelastic effect.

Since the partial derivative of the refractive index taken at zero stress, $\left(\frac{\partial n}{\partial T} \right)_{\sigma=0}$, was measured directly in the published data, the following relation should be used [25]:

$$\left(\frac{\partial n}{\partial T} \right)_{\epsilon=0} (T) = \left(\frac{\partial n}{\partial T} \right)_{\sigma=0} (T) + \frac{\alpha_T(T) \cdot n_0^3}{2} (p_{11} + 2p_{12}), \tag{3}$$

where p_{11} and p_{12} are the coefficients related to the components of a fourth-rank elasto-optical tensor. The population of the excited laser state can be easily obtained from the experimentally investigated gain coefficient $G(x, y)$ [26]:

$$G(x, y) = \exp[L \cdot \sigma_L(T)(N(x, y) \cdot f_{11}(T) - (N_{tot} - N(x, y)) \cdot f_{03}(T))], \quad (4)$$

where $\sigma_L(T)$ is the luminescence cross-section at the gain wavelength, m^2 ; N_{tot} is the dopant ion concentration, ions/ m^3 ; and $f_{11}(T)$ and $f_{03}(T)$ are Boltzmann occupation factors.

In formulae (1)–(4), the dependence of laser and thermophysical parameters of a gain medium is taken into account. Generally, elasto-optical coefficients p_{ij} and, calculated from them, photoelastic constants $C_{r,\theta}$ are temperature-dependent [27]. But, according to our knowledge, there are no measurements of temperature dependence or even values of elasto-optical coefficients at cryogenic temperatures for Yb:YAG crystals or ceramics. So, in our calculations, we used elasto-optical coefficients and photoelastic constants determined at room temperature. There was a polarizability difference Δp at room temperatures [28] and cryogenic temperatures [29] in earlier published data, and the values differed by approximately 2 times. Thus, the polarizability difference is strongly dependent on the temperature value. To the best of our knowledge, there are no published data concerning the dependence of the polarizability difference on temperature. So, it is considered as a constant, and the value $88 \times 10^{-34} m^2$ reported in [29] was used.

The distributions of temperature and population density of the excited laser state were determined experimentally in the pump region in accordance with the laser scanning technique developed by the authors. The method is a development of the previously reported method for studying the temperature in the active elements of laser amplifiers [22]. The method allows one to carry out a simultaneous experimental investigation of temperature and population density based on measuring the transmittance and gain in the active element. The method can be used in the case of an active medium in which the absorption cross-section at the gain wavelength is temperature-dependent. However, if it is necessary to measure only the temperature distribution, it is sufficient if a temperature dependence of the absorption cross-section at the wavelength of the scanning laser is present.

The experimental setup for scanning an active element is shown in Figure 1.

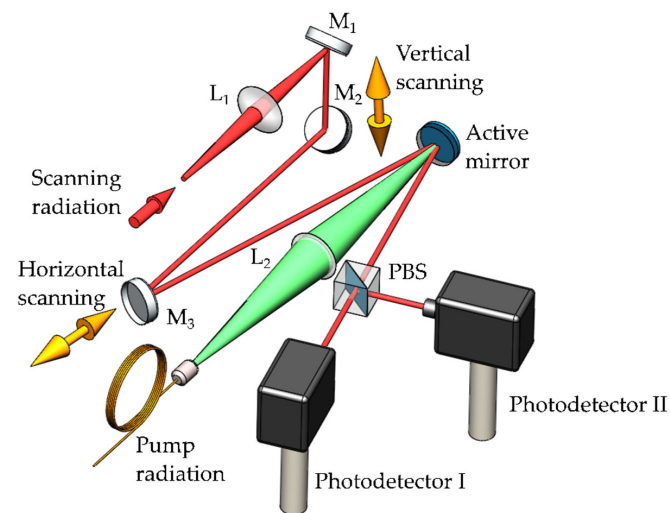


Figure 1. Experimental setup for scanning an active element. M_1 , M_2 , M_3 are flat mirrors; L_1 , L_2 are focusing lenses; PBS stands for polarizing beamsplitter; photodetectors I, II are large-aperture photodiode-based detectors.

Such an experimental setup can be used for different geometries of active elements, including active mirrors and slabs. In the experiment, the laser radiation at the gain wavelength was focused into an active element and translated in parallel by movable mirrors M_2 and M_3 to scan a certain region in the active element. The radiation passed

through the lens (L_1) before being reflected by the mirrors for scanning. The first mirror (M_2) displaced the beam in the vertical direction, and the second one (M_3), in the horizontal direction. The horizontal plane was parallel to the plane of the optical table. To accelerate the scanning process, the motion of translation stages, on which mirrors were mounted, was automated. The setup also contained a CCD camera to monitor the stability of the beam position during scanning and a photodetector to monitor the scanning radiation power. A polarizing beamsplitter (PBS), photodetector I, and photodetector II were used to measure the change in the polarization of scanning radiation in an active element (described in the section titled Results). For the measurement of temperature and gain coefficient, the experimental setup without the PBS and photodetector II was used. Such a measurement can be carried out using a CCD camera [30] and a large-diameter probe beam without scanning. In this case, the wavefront distortion introduced by an active element and entire optic system affected the measured absorption and gain profiles. So, laser scanning allows one to measure the temperature and gain coefficient profiles without the influence of wavefront distortions. Also, a CCD camera typically has a much lower temporal resolution compared to photodiode-based detectors.

The investigation algorithm was as follows. The transmittance coefficient dependence on the active element temperature was investigated in the absence of pump radiation $k(T) = \frac{P_I(T)}{P_c}$, where P_I and P_c are the radiation power measured by the photodetector I and control photodetector, respectively. The dependence $T(k)$ was then calculated from it.

So, since not only the active element was scanned by the laser beam but also the mirrors, lens, and the photosensitive active regions of the photodetector, it was necessary to take into account temperature-independent losses in the optic system. For this purpose, the transmittance coefficient distribution was measured in a cooled active element without pumping, $k(T = T_c, x, y)$.

Consider the situation when the active element is pumped. In the case of a high pulse repetition rate or large duty cycle, the upper laser level does not have time to completely decay between pump pulses. If so, the pump radiation should be interrupted for a period several times longer than the lifetime of the upper-level state. This allows one to measure the absorption coefficient not affected by the pumping radiation. Since the average radiation power decreases when the pump radiation is interrupted, the pump interruption frequency should be chosen so as to have a minimal effect on the steady-state temperature field in the active element. In our studies, the pumping process was interrupted 2 times per second for 10 ms, and it corresponded to a decrease in the average pump radiation power by 2%. The transmittance distribution $k_p(x, y)$ and gain distribution $k_g(x, y)$ in the active element were investigated. A typical signal in the vicinity of a pump interruption is shown in Figure 2. In this case, pump pulses had a repetition rate of 1 kHz and pulse duration 0.6 ms. The scanning radiation was continuous wave. To avoid numerical errors, the signal was fitted with a decaying exponent.

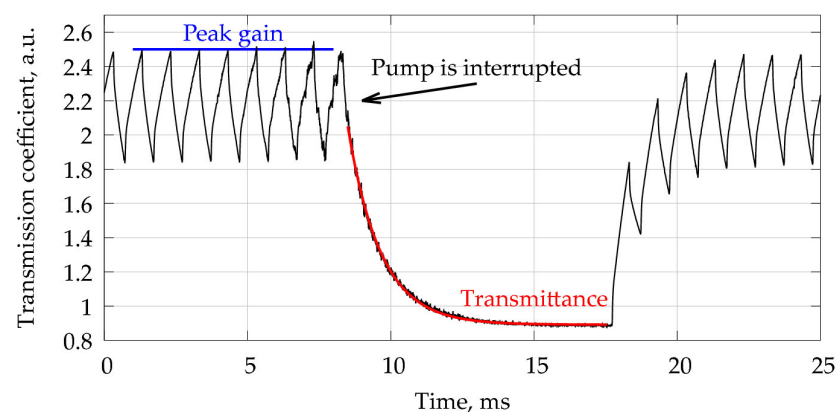


Figure 2. Dynamics of the radiation transmission coefficient.

The investigated distributions were divided to the transmittance distribution in the cooled active element (from step 2), $K(x, y) = \frac{k_p(x, y)}{C(x, y)}$ and $G = \frac{k_g(x, y)}{C(x, y)}$, where $C = k(T = T_c, x, y)$. The equivalent temperature was determined from the measured transmittance using the dependence $T(k)$ (from step 1). The equivalent temperature was the temperature of the uniformly heated active element with the same transmittance as the measured one [22]. The temperature dependence of the absorption coefficient in the element is specified as follows:

$$A(T) = \exp(-\alpha(T) \cdot L). \tag{5}$$

Then, the equivalent temperature is:

$$T_c = A^{-1}(A), \tag{6}$$

where A^{-1} is the inverse function of A .

For an arbitrary temperature distribution and absorption coefficient temperature dependence, the equivalent temperature T_c and average temperature T_a are different. If the temperature is constant along the z -axis in the active element, then T_c and T_a are the same. Moreover, if absorption depends linearly on temperature, the quantities are also the same regardless of the temperature distribution. Let the absorption coefficient per unit length to be written as $\alpha(T) = a + b \cdot T$, where a, b are arbitrary real-valued coefficients. Then, the absorption in the element over the path L is

$$\exp\left(-\int_0^L \alpha(T(z)) dz\right) = \exp\left(-a \cdot L - b \int_0^L T(z) dz\right) = \exp(-L \cdot (a + b \cdot T_a)) \equiv A(T_a). \tag{7}$$

This relation is held for an arbitrary temperature distribution.

In case the absorption coefficient does not comply with the linearity requirement, then the equivalent temperature, as well as the average temperature, lies in the range between minimum and maximum temperatures. In the Yb:YAG crystal, there was an almost linear region of the absorption coefficient (Figure 3).

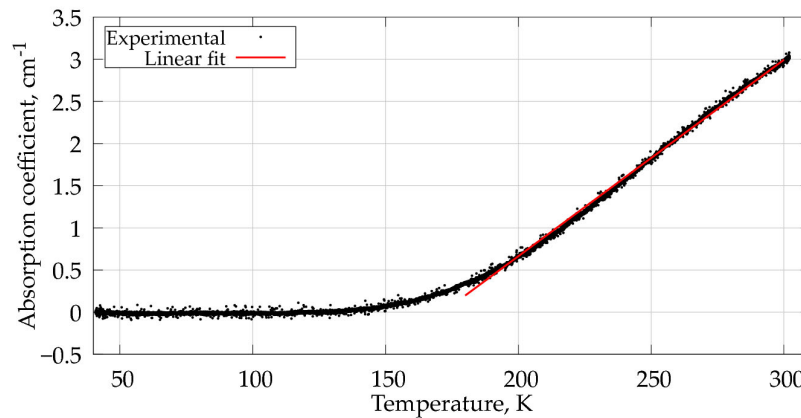


Figure 3. Dependence of absorption coefficient on temperature, as measured in Yb:YAG (doping level 9.8 at.%).

As can be seen, for the temperature values in the range of 180–280 K, the dependence was almost linear and the maximal relative error of fit was less than 7%. In this region, the temperature measured by the laser scanning method was, therefore, the average temperature, which was conventionally used to calculate the wavefront distortion.

The uncertainty was calculated by the means of error propagation formula:

$$\Delta_T = \frac{1}{C} \left| \frac{\partial T(k)}{\partial k} \right| \sqrt{(\sigma_k)^2 + (K \cdot \sigma_C)^2} \cdot t_s, \tag{8}$$

$$\Delta_G = \frac{1}{C} \sqrt{(\sigma_g)^2 + (K \cdot \sigma_C)^2} \cdot t_s, \quad (9)$$

where σ_k is the transmittance standard deviation, σ_C is the standard deviation of the transmittance measured in the absence of pump radiation, σ_g is the standard deviation of the gain coefficient, and t_s is the coefficient calculated using the Student distribution with a 97.5% confidence interval. To determine the number of repeated measurements at each point on the map, the dependence of the error in determining the temperature on the number of transmittance measurements in different regions of the active element was estimated in different map points. A typical dependence is presented in Figure 4.

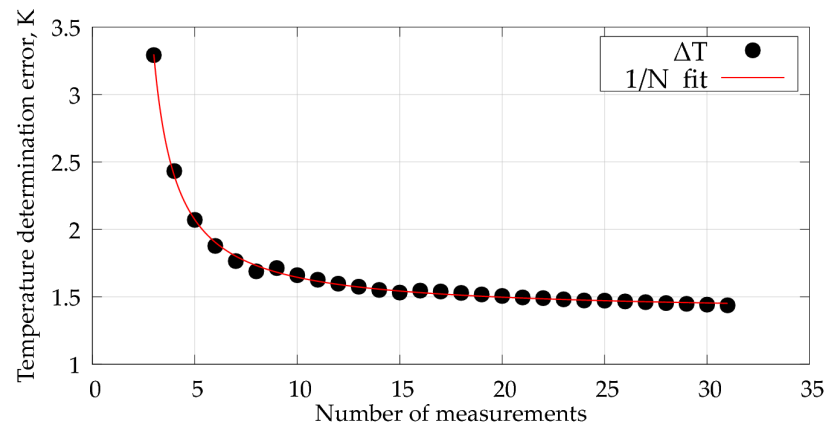


Figure 4. Dependence of the temperature determination error on the number of transmittance measurements.

The error in temperature determining decreased as $1/N$, where N is the number of measurements. For the measurement presented in the graph, the minimum value of the temperature determination error based on the curve fitting results was 1.37 K. The non-zero limit value was due to the influence of the instrumental error of the recording system. In our study, the number of repeated measurements was chosen to be 15. Therefore, the degree of freedom used for the calculation was 14 for the temperature measurements. The number of peak gain coefficient measurements in a single map point was more than 10,000.

3. Results

To verify the method, the study of the amplified radiation wavefront distortion was carried out. The distortion was measured in one of the eight active elements of a 16-pass laser amplifier with cryogenic cooling and an average pump radiation power of up to 200 W [13]. The active elements were diffusion-bonded, disk-shaped YAG-Yb:YAG crystals (Yb^{3+} ion concentration 9.8 at.%), which were attached in pairs on the opposite sides to cryogenically cooled copper holders. The disk diameter was 25.4 mm, the thickness of the doped part was 3.75 mm, and the thickness of the undoped part was 2 mm. During the laser scanning, absorption and amplification occurred only in the doped part. Accordingly, when calculating the OPD, the optical radiation path length was taken into account only in the doped part. The undoped part did not affect the electronic component of the OPD due to the lack of an upper-level population distribution. According to the simulated data, the temperature distribution in the undoped part had significantly smaller gradients in comparison with the doped part, and, therefore, it induced a negligible effect on the result of the OPD calculation.

A continuous wave laser with a central wavelength of 1030 nm and a spectral width of less than 0.3 nm was used for scanning. The beam diameter in the active element was $220 \pm 14 \mu\text{m}$. The angle between the direction of propagation of the scanning radiation and the normal to the surface was 9.5° in the horizontal plane. The pump beam had a hyper-Gaussian intensity profile, the pump beam diameter was 2 mm ($1/e^2$ level), pump pulses had a square shape in the time domain, the pulse repetition rate was 1000 Hz, the

peak power was 180 W, the average absorbed power of the pump radiation was 110 W, and the duty cycle was 60%. The experimental scheme is shown in Figure 1.

The field with a diameter of 4.4 mm was scanned. The maximum measured temperature was 192 ± 0.6 K, and the temperature at the edges of the scanned area was ~ 165 K. The error in determining the temperature did not exceed 2.5 K. The maximum gain was 2.9 ± 0.07 , and the error in determining the gain did not exceed 0.09. The thermal contribution determination error took into account the temperature determination error. The electronic contribution was calculated using the temperature error as well as the gain coefficient error. In Figure 5A,B are the thermal and electronic contributions to the OPD profile introduced by the active element. The corresponding horizontal sections of the OPD are represented in Figure 5C,D, respectively.

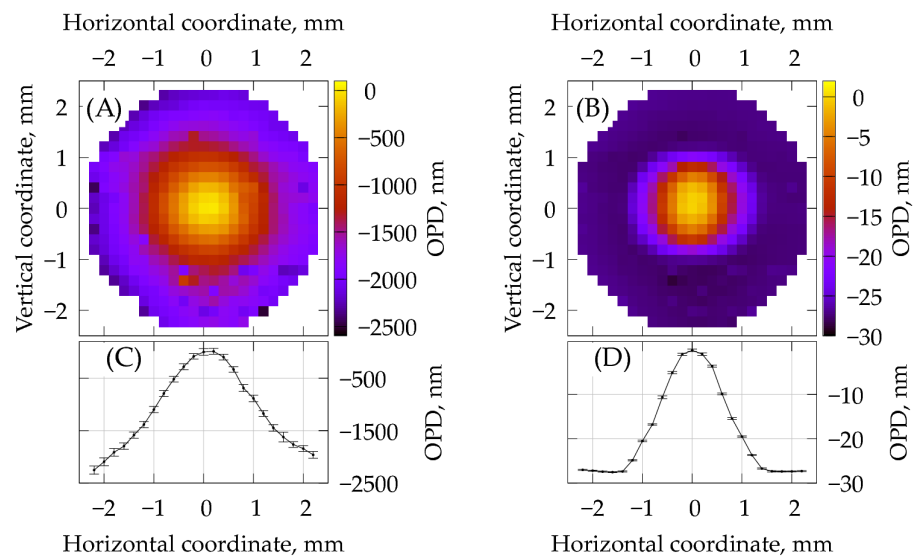


Figure 5. Contributions to the OPD profile: (A) thermal (radial polarization), (B) electronic, OPD profiles in the horizontal cross-section (C) for thermal contribution and (D) for electronic contribution.

The electronic contribution to the OPD was less than the temperature contribution by 2 orders of magnitude, which was in agreement with the data available for laser systems with a high average power [21,29]. For systems with low pulse repetition rates and high peak power, the electronic contribution to the wavefront distortion was comparable to the thermal contribution and may even have exceeded it [18].

The OPD profiles were analyzed using Zernike polynomials. The thermal profile of the OPD was defined mostly by the following terms: vertical tilt, 51.1 nm; defocus, 498.2 nm; primary spherical aberration, 171.4 nm; and second spherical aberration, 65.5 nm. The electronic profile was almost not tilted; so, the next terms were significant in the electronic profile: defocus, 4.9 nm; primary spherical aberration, 4.2 nm; and second spherical aberration, 2.2 nm. Since the OPD contained significant high-order coefficients, namely, the second spherical aberration, the equivalent focal length estimated using Zernike coefficients could have been inaccurate. To determine the focal length of the thermal and electron lenses, the corresponding contributions to the OPD were considered as the effect of a thin spherical lens and approximated by an elliptic paraboloid in the region limited by the pump beam diameter of 2 mm. Thus, the focal lengths of the thermal lens were $f_x = 0.40 \pm 0.03$ m and $f_y = 0.47 \pm 0.05$ m, and the focal lengths of the electronic length were estimated to be $f_x = 21.3 \pm 1.9$ m and $f_y = 20.9 \pm 1.7$ m. For the thermal OPD profile, the equivalent focal length calculated according to [31] was two times larger than one calculated by means of a parabolic approximation.

It is known that the laser and thermal characteristics of Yb:YAG are strongly dependent on temperature. Therefore, in the case of a large temperature gradient, the accounting for this dependence becomes necessary, especially for the electronic contribution to the

wavefront distortion. The influence of temperature-dependent parameters' distribution on the determination of the OPD profile was analyzed. The thermal and electronic contributions introduced by the active element were calculated for the case of distributed medium parameters and for the case of the parameters taken at the minimal measured temperature of 165 K. The thermal contributions calculated in these ways were slightly different. The maximal difference between the calculated profiles was 57.5 nm, which was 2 orders lower than the amplitude of thermal contribution to the OPD profile. For the electronic contribution, the neglect of temperature dependence resulted in a more significant error. The difference in the calculated profiles increased from the center to the edges to 5.6 nm, which corresponded to a decrease in amplitude by 20% without taking into account the temperature dependence.

The difference between the thermal contribution to the OPD profile for radial and tangential polarizations, calculated from formula (1) $\delta = \Delta l_r - \Delta l_\theta$, increased from the center of the active element to the edge, from 0 nm to 150 nm, which was an order of magnitude smaller than the amplitude of the thermal contribution. The maximal error in determining the difference between the OPD for different polarizations was 10.5 nm. In the Yb:YAG case, for the radial polarization, the photoelastic effect contributed to the OPD with the same sign as other mechanisms, forming a positive lens; for the tangential component, it had a different sign. The difference in the OPD for the radial and tangential polarizations led to the radiation depolarization effect [8,9]. A thermally induced stress led to the birefringence due to the photoelastic effect. Radiation, passing through various regions of the active element, was decomposed into radial and tangential polarizations. The directions of the vectors, along which the radiation was decomposed, the phase difference and, consequently, the polarization of the radiation that passed through the active element, had spatial distributions. The depolarization effect is especially detrimental in cases where polarization-sensitive elements are used in laser systems. To calculate the radiation depolarization, the active element was considered as a set of wave plates, the action of which can be described by Jones matrices [32] (p. 447).

The depolarization of radiation was calculated from the difference in the OPD for the radial and tangential components and measured experimentally by the setup shown in Figure 1. The fraction of radiation power with a polarization state orthogonal to the initial state was determined (hereinafter, the fraction of depolarized radiation). For the measurement, incident radiation was horizontally polarized, and a polarizing beamsplitter was introduced into the radiation passed through the active element. The beamsplitter with a transmitted beam extinction ratio of 1000:1 and reflected beam extinction ratio of 100:1 was used. The power of the beams after the beamsplitter was measured. The fraction of depolarized radiation was determined as $\frac{P'_y}{P'_x + P'_y}$, where $P'_{x,y}$ is the power of the horizontal and vertical polarizations. The depolarization of radiation caused by constant stresses was measured in the cooled active element without pumping radiation. The depolarization in the absence of pumping was no more than a half percent. In Figure 6 are the calculated and measured maps of the fraction of depolarized radiation.

The maximal value of the fraction of depolarized radiation calculated from the OPD profiles was 18.3%. For the experimentally measured radiation depolarization profile, the maximal value was 17.9%. Thus, the results were in a good agreement. A slight difference in the profile shapes may have been caused by the fact that the calculation did not take into account the angle between the direction of propagation of the scanning radiation and the normal to the surface of the active element. In the region limited by the pump beam diameter of 2 mm, the maximum value of the experimentally measured fraction of depolarized radiation was 8.5%. This confirmed that it is necessary to take into account the depolarization of radiation and compensate for this effect in a 16-pass laser amplifier.

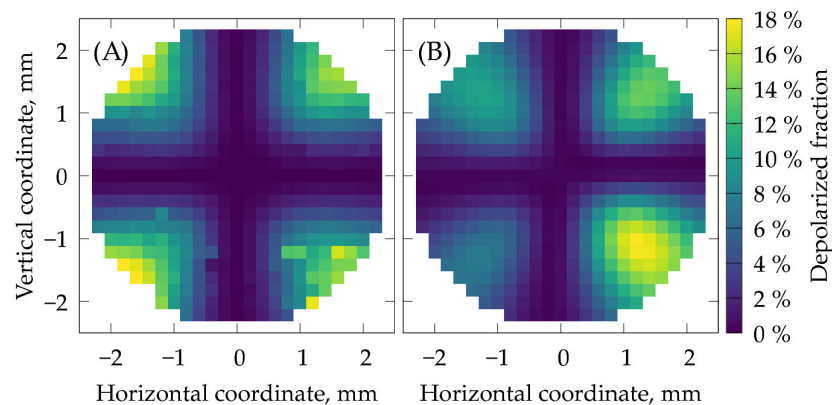


Figure 6. The fraction of depolarized radiation: (A) calculated from the difference in OPD for radial and tangential polarizations; (B) measured experimentally.

4. Conclusions

A novel, noncontact optical method was proposed for a time-resolved simultaneous measurement of the temperature distribution and population density of the excited laser state. This method was used to study the thermal and electronic contributions to the wavefront distortion and radiation depolarization in the Yb:YAG active element of a cryogenically cooled laser amplifier with a high-power diode pumping. The focal length of the thermal lens was 0.40 ± 0.03 m and 0.47 ± 0.05 m for the horizontal and vertical planes, respectively. The focal length of the electron lens was two orders of magnitude larger, and it was equal to 21.3 ± 1.9 m and 20.9 ± 1.7 m for the horizontal and vertical planes, respectively. It was shown that, with a small modification in the experimental setup, it is also possible to carry out direct experimental measurements of the thermally induced depolarization of radiation. The maximal value of the radiation power losses induced by depolarization in the region limited by the pump beam diameter was 8.5%. The directly measured depolarization of radiation confirmed the result of the OPD investigation.

The advantages of the method include the simultaneous study of the active medium parameters at the amplification wavelength. This feature provides a possibility to separately verify theoretical models for both contributions to the wavefront distortion. Such a possibility is especially valuable for high peak power laser systems, where an electronic contribution may be high enough. Also, the method opens the way to verify the theoretical models of temperature and population density distributions. With such verified models, one can calculate the wavefront distortion using any suitable approximation for specific experimental conditions. Another advantage of the method is the application of photodiode-based detectors, which allow reaching a high time resolution. The method is simple and does not require a high stability and quality of the radiation wavefront and intensity distribution. The spatial resolution of the method can be increased by focusing radiation more tightly into the active element. The method can be used in the case of any active medium in which the absorption cross-section at the gain wavelength is temperature-dependent.

Author Contributions: Conceptualization, V.A.P. and V.V.P.; methodology, V.V.P. and V.V.A.; software, A.O.K. and G.V.K.; investigation, A.O.K. and G.V.K.; data curation, V.A.P. and G.V.K.; writing—original draft preparation, A.O.K., G.V.K., and V.A.P.; writing—review and editing, V.V.P. and V.V.A.; validation, V.V.A.; visualization, G.V.K. and A.O.K.; supervision, V.V.P. All authors have read and agreed to the published version of the manuscript.

Funding: The reported study was funded by the Russian Science Foundation, grant No. 23-22-00238.

Institutional Review Board Statement: Not applicable.

Informed Consent Statement: Not applicable.

Data Availability Statement: Data are available from the authors on request.

Conflicts of Interest: The authors declare no conflicts of interest. The funder had no role in the design of the study; in the collection, analyses, or interpretation of data; in the writing of the manuscript; or in the decision to publish the results.

References

1. Song, J.; Peng, Y.; Shen, L.; Sun, J.; Luo, G.; Xu, X.; Xu, J.; Leng, Y. High-power femtosecond regenerative amplifier based on Yb:CaYAlO₄ dual-crystal configuration. *Opt. Lett.* **2023**, *48*, 1395–1398. [[CrossRef](#)] [[PubMed](#)]
2. Mironov, E.A.; Kuznetsov, I.I.; Palashov, O.V.; Morozov, O.A.; Naumov, A.K. Broadband amplification and thermal lensing in a combination of Yb:YLF and Yb:YAG crystals. *Appl. Opt.* **2024**, *63*, 4508–4517. [[CrossRef](#)]
3. Eckold, M.; Mackenzie, J.I.; Clarkson, W.A. Approach for power scaling solid-state lasers with intracavity motion. *Opt. Lett.* **2017**, *42*, 775–778. [[CrossRef](#)] [[PubMed](#)]
4. Sekine, T.; Kurita, T.; Hatano, Y.; Muramatsu, Y.; Kurata, M.; Morita, T.; Watari, T.; Iguchi, T.; Yoshimura, R.; Tamaoki, Y.; et al. 253 J at 0.2 Hz, LD pumped cryogenic helium gas cooled Yb:YAG ceramics laser. *Opt. Express.* **2022**, *30*, 44385–44394. [[CrossRef](#)] [[PubMed](#)]
5. Petrov, V.A.; Kuptsov, G.V.; Kuptsova, A.O.; Atuchin, V.V.; Stroganova, E.V.; Petrov, V.V. Enhanced Yb:YAG Active Mirrors for High Power Laser Amplifiers. *Photonics* **2023**, *10*, 849. [[CrossRef](#)]
6. Chénais, S.; Balembois, F.; Druon, F.; Lucas-Leclin, G.; Georges, P. Thermal lensing in diode-pumped ytterbium Lasers-Part I: Theoretical analysis and wavefront measurements. *IEEE J. Quantum Electron.* **2004**, *40*, 1217–1234. [[CrossRef](#)]
7. Chénais, S.; Balembois, F.; Druon, F.; Lucas-Leclin, G.; Georges, P. Thermal lensing in diode-pumped ytterbium Lasers-Part II: Evaluation of quantum efficiencies and thermo-optic coefficients. *IEEE J. Quantum Electron.* **2004**, *40*, 1235–1243. [[CrossRef](#)]
8. De Vido, M.; Mason, P.D.; Fitton, M.; Eardley, R.W.; Quinn, G.; Clarke, D.; Ertel, K.; Butcher, T.J.; Phillips, P.J.; Banerjee, S.; et al. Modelling and measurement of thermal stress-induced depolarisation in high energy, high repetition rate diode-pumped Yb:YAG lasers. *Opt. Express.* **2021**, *29*, 5607–5623. [[CrossRef](#)]
9. Veselis, L.; Burokas, R.; Ulčinas, O.; Gertus, T.; Michailovas, K.; Michailovas, A. Depolarization compensation with a spatially variable wave plate in a 116 W, 441 fs, 1 MHz Yb:YAG double-pass laser amplifier. *Appl. Opt.* **2021**, *60*, 7164–7171. [[CrossRef](#)]
10. Yoon, J.W.; Kim, Y.G.; Choi, I.W.; Sung, J.H.; Lee, H.W.; Lee, S.K.; Nam, C.H. Realization of laser intensity over 10²³ W/cm². *Optica* **2021**, *8*, 630–635. [[CrossRef](#)]
11. Guo, Z.; Yu, L.; Wang, J.; Wang, C.; Liu, Y.; Gan, Z.; Li, W.; Leng, Y.; Liang, X.; Li, R. Improvement of the focusing ability by double deformable mirrors for 10-PW-level Ti: Sapphire chirped pulse amplification laser system. *Opt. Express.* **2018**, *26*, 26776–26786. [[CrossRef](#)] [[PubMed](#)]
12. Zhao, Z.; Gao, Y.; Cui, Y.; Xu, Z.; An, N.; Liu, D.; Wang, T.; Rao, D.; Chen, M.; Feng, W.; et al. Investigation of phase effects of coherent beam combining for large-aperture ultrashort ultrahigh intensity laser systems. *Appl. Opt.* **2015**, *54*, 9939–9948. [[CrossRef](#)]
13. Petrov, V.V.; Petrov, V.A.; Kuptsov, G.V.; Laptev, A.V.; Kirpichnikov, A.V.; Pestyakov, E.V. Modelling of the laser amplification process with allowance for the effect of the temperature distribution in an Yb:YAG gain element on the thermophysical and lasing characteristics of the medium. *Quantum Electron.* **2020**, *50*, 315–320. [[CrossRef](#)]
14. Shayeganrad, G. Experimental study of variable thermal lens in a two-stage chirped-pulse high-power Ti:sapphire amplifier at 1kHz. *Optik* **2018**, *174*, 715–726. [[CrossRef](#)]
15. Furuse, H.; Sakurai, T.; Chosrowjan, H.; Kawanaka, J.; Miyanaga, N.; Fujita, M.; Ishii, S.; Izawa, Y. Amplification characteristics of a cryogenic Yb³⁺:YAG total-reflection active-mirror laser. *Appl. Opt.* **2014**, *53*, 1964–1969. [[CrossRef](#)] [[PubMed](#)]
16. Starikov, F.A.; Kochemasov, G.G.; Kulikov, S.M.; Manachinsky, A.N.; Maslov, N.V.; Ogorodnikov, A.V.; Sukharev, S.A.; Aksenov, V.P.; Izmailov, I.V.; Kanev, F.Y.; et al. Wavefront reconstruction of an optical vortex by a Hartmann–Shack sensor. *Opt. Lett.* **2007**, *32*, 2291–2293. [[CrossRef](#)] [[PubMed](#)]
17. Chanteloup, J.-C. Multiple-wave lateral shearing interferometry for wave-front sensing. *Appl. Opt.* **2005**, *44*, 1559–1571. [[CrossRef](#)] [[PubMed](#)]
18. Tamer, I.; Keppler, S.; Hornung, M.; Körner, J.; Hein, J.; Kaluza, M.C. Spatio-Temporal Characterization of Pump-Induced Wavefront Aberrations in Yb³⁺-Doped Materials. *Laser Photonics Rev.* **2018**, *12*, 1700211. [[CrossRef](#)]
19. Yu, Y.; Di, J.; Qu, W.; Asundi, A. Measurement of thermal effects of diode-pumped solid-state laser by using digital holography. *Appl. Opt.* **2018**, *57*, 5385–5391. [[CrossRef](#)]
20. Shimansky, R.V.; Belousov, D.A.; Korolkov, V.P.; Kuts, R.I. Diffractive Sensor Elements for Registration of Long-Term Instability at Writing of Computer-Generated Holograms. *Sensors* **2021**, *21*, 6635. [[CrossRef](#)]
21. Chi, H.; Baumgarten, C.M.; Jankowska, E.; Dehne, K.A.; Murray, G.; Meadows, A.R.; Berrill, M.; Reagan, B.A.; Rocca, J.J. Thermal behavior characterization of a kilowatt-power-level cryogenically cooled Yb:YAG active mirror laser amplifier. *J. Opt. Soc. Am. B* **2019**, *36*, 1084–1090. [[CrossRef](#)]
22. Kuptsov, G.V.; Konovalova, A.O.; Petrov, V.A.; Laptev, A.V.; Atuchin, V.V.; Petrov, V.V. Laser Method for Studying Temperature Distribution within Yb:YAG Active Elements. *Photonics* **2022**, *9*, 805. [[CrossRef](#)]
23. Chénais, S.; Druon, F.; Forget, S.; Balembois, F.; Georges, P. On thermal effects in solid-state lasers: The case of ytterbium-doped materials. *Prog. Quantum Electron.* **2006**, *30*, 89–153. [[CrossRef](#)]

24. Anashkina, E.; Antipov, O. Electronic (population) lensing versus thermal lensing in Yb:YAG and Nd:YAG laser rods and disks. *J. Opt. Soc. Am. B* **2010**, *27*, 363–369. [[CrossRef](#)]
25. Dement'ev, A.S. Relationships between different expressions of thermo-optic and photoelastic coefficients of YAG crystal. *Laser Phys.* **2015**, *25*, 095004. [[CrossRef](#)]
26. Petrov, V.A.; Petrov, V.V.; Kuptsov, G.V.; Laptev, A.V.; Galutskiy, V.V.; Stroganova, E.V. YAG:Yb crystal with non-linear doping ions distribution as promising active element for high average power laser systems. *Laser Phys.* **2021**, *31*, 035003. [[CrossRef](#)]
27. Mukhin, I.B.; Palashov, O.V.; Khazanov, E.A.; Vyatkin, A.G.; Perevezentsev, E.A. Laser and thermal characteristics of Yb:YAG crystals in the 80–300 K temperature range. *Quantum Electron.* **2011**, *41*, 1045–1050. [[CrossRef](#)]
28. Moncorge, R.; Eremeykin, O.N.; Doualan, J.L.; Antipov, O.L. Origin of athermal refractive index changes observed in Yb³⁺ doped YAG and KGW. *Opt. Commun.* **2008**, *281*, 2526–2530. [[CrossRef](#)]
29. Kilinc, M.; Demirbas, U.; Gonzalez-Diaz, J.B.; Thesinga, J.; Kellert, M.; Palmer, G.; Kärtner, F.X.; Pergament, M. Thermal and population lensing of Yb:YLF at cryogenic temperature. *Opt. Mater. Express.* **2023**, *13*, 3200–3216. [[CrossRef](#)]
30. Körner, J.; Yue, F.; Hein, J.; Kaluza, M.C. Spatially and temporally resolved temperature measurement in laser media. *Opt. Lett.* **2016**, *41*, 2525–2528. [[CrossRef](#)]
31. Mafusire, C.; Forbes, A. Mean focal length of an aberrated lens. *J. Opt. Soc. Am. B* **2008**, *28*, 1403–1409. [[CrossRef](#)] [[PubMed](#)]
32. Mezenov, A.V.; Soms, L.N.; Stepanov, A.I. Thermo-optics of solid-state lasers. *J. Russ. Laser Res.* **1987**, *8*, 427–549. [[CrossRef](#)]

Disclaimer/Publisher's Note: The statements, opinions and data contained in all publications are solely those of the individual author(s) and contributor(s) and not of MDPI and/or the editor(s). MDPI and/or the editor(s) disclaim responsibility for any injury to people or property resulting from any ideas, methods, instructions or products referred to in the content.